

Nanoscopic coexistence of magnetism and superconductivity in $\text{YBa}_2\text{Cu}_3\text{O}_{6+x}$ detected by μSR .

S. Sanna,¹ G. Allodi,² G. Concas,¹ A. D. Hillier,³ and R. De Renzi²

¹*Dipartimento di Fisica e Unità INFN di Cagliari, I 09042 Monserrato (Ca), Italy*

²*Dipartimento di Fisica e Unità INFN di Parma, I 43100 Parma, Italy*

³*ISIS Muon Facility, Rutherford Appleton Laboratory, Chilton, OX11 0QX, United Kingdom*

(Dated: December 2, 2024)

We performed zero and transverse field μSR experiments on a large number of $\text{YBa}_2\text{Cu}_3\text{O}_{6+x}$ samples. We detect coexistence of antiferro-type (AF) short range magnetism with superconductivity below $T_f \lesssim 10$ K in compositions $0.37 \lesssim x \lesssim 0.39$. Most muons experience local AF fields, even when SQUID detects a full superconducting volume fraction, which points to a local *minimal interference* organization of short AF stripes embedded in the superconductor. A detailed phase diagram is produced and the consequences of the minimal interference are discussed.

The appearance of low temperature magnetism in low doping cuprate superconductors was an early μSR claim [1] for $\text{YBa}_2\text{Cu}_3\text{O}_{6+x}$, later reproduced [2] in $\text{La}_{2-x}\text{Sr}_x\text{CuO}_4$, but initially highly disputed [3, 4]. More recently it has been established that superconducting $\text{Y}_{1-y}\text{Ca}_y\text{Ba}_2\text{Cu}_3\text{O}_{6+x}$ [5], $\text{Ca}_{1-x}\text{La}_x\text{Ba}_{2-y}\text{La}_y\text{Cu}_3\text{O}_{6+z}$ [6, 7], $\text{La}_{2-x}\text{Sr}_x\text{Cu}_{1-y}\text{Zn}_y\text{O}_4$ [8] and $\text{La}_{2-x}\text{Sr}_x\text{CuO}_4$ [9] exhibit magnetic order. Zero field μSR detects internal spontaneous magnetic fields \mathbf{B}_i in sizeable volume fractions of samples which display bulk superconductivity (SC). In a few cases the whole volume is involved, i.e. all implanted muons experience internal fields.

Neutron scattering also detects magnetic correlations, notably [10] in $\text{YBa}_2\text{Cu}_3\text{O}_{6.35}$, exclusively dynamic in nature, although their static counterpart could be elusive due to a very short range. The doubled magnetic unit cell indicates an antiferromagnetic (AF) structure, with a suggested stripe-like character.

In all the samples explored so far by μSR [5, 6, 7, 8, 9] it has been hinted that the cluster spin glass nature of their magnetism (low spin freezing temperature, T_f , large distributions of \mathbf{B}_i and absence of long range order as from neutron diffraction [11, 12]) might be favoured by the disorder inherent in cation substituted perovskites, which directly influences the CuO_2 layers. Conversely in $\text{YBa}_2\text{Cu}_3\text{O}_{6+x}$ the source of disorder, namely the basal CuO_x layers, are farther removed from the CuO_2 layers. However, systematic data on this classical cuprate system, besides the early ones of Ref. 1, are lacking. This motivates the present work, which has the purpose of clarifying whether the appearance of coexisting superconducting and magnetic properties is indeed intrinsic to the unperturbed underdoped CuO_2 layers and whether the two properties cooperate or interfere.

We performed μSR measurements on twenty-four polycrystalline $\text{YBa}_2\text{Cu}_3\text{O}_{6+x}$ samples (Y_{1-24}) prepared by the topotactic technique, which consists in oxygen equilibration of stoichiometric quantities of the two end member specimen, tightly packed in sealed vessels [13]. Low temperature annealing yields high quality homogeneous

samples with an absolute error of $\delta x = \pm 0.02$ in oxygen content per formula unit and a much smaller relative error between samples of the same batch. The hole content h was determined from the resistive T_c for the superconducting samples [14], and from the Seebeck coefficient S at 290 K for the non-superconducting ones, using the exponential dependence [14] of S on h , with fit parameters determined from our series of samples [21].

Samples Y_{1-8} , with oxygen content $0.20 \leq x \leq 0.32$ and hole content per planar Cu atom $0.033 \leq h \leq 0.055$, never superconduct, and their AF properties were reported previously [15]. Samples Y_{9-24} , with $0.32 \leq x \leq 0.42$ and $0.055 \leq h \leq 0.08$, are superconductors and are the subject of the present work.

The μSR experiment were performed on the MUSR spectrometer of the ISIS pulsed muon facility, where the external magnetic field \mathbf{H} may be applied either parallel to the initial muon spin \mathbf{S}_μ , in longitudinal (LF) or perpendicular to \mathbf{S}_μ , in transverse field (TF) experiments. The LF detector setup is used also in zero field (ZF) experiments.

The asymmetry in the muon decay is always obtained from the count rates N_i in two sets of opposite detectors as $\mathcal{A}(t) = [N_1(t) - \alpha N_2(t)]/[N_1(t) + \alpha N_2(t)]$; the effective relative count efficiency α is calibrated at high temperature.

The spin precessions around the local field $\mathbf{B}_\mu = \mu_0(\mathbf{H} + \mathbf{M}_\mu)$ yields a TF asymmetry as $\mathcal{A}_T(t) = a_{TF} G_{xx}(t) \cos(2\pi\gamma B_\mu t)$, where a_{TF} is the amplitude, $\gamma = 135.5$ MHz/T is the muon gyromagnetic ratio and G_{xx} the transverse muon relaxation function, i.e. the time decay of the precession. Superconducting and magnetically ordered phases give rise to a different local magnetization \mathbf{M}_μ , hence to distinctive features in G_{xx} . The amplitudes of these distinctive signals are directly proportional to the volume fraction where the corresponding order parameter is established.

The ZF asymmetry in the paramagnetic phase is $\mathcal{A}_Z(t) = a_{ZF} G_{zz}(t)$, where the weak longitudinal relaxation G_{zz} originates from the nuclear dipolar fields. No

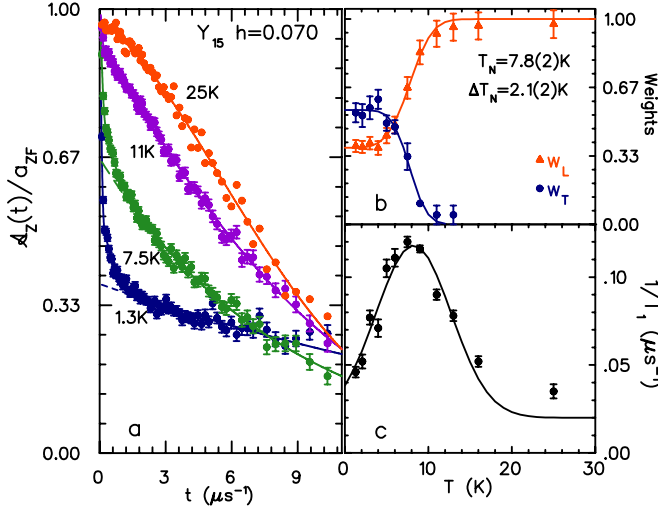


FIG. 1: ZF μ SR, sample Y₁₅ a) Normalized asymmetries at $T/T_N \approx 0.17, 0.96, 1.4, 3.2$; b) longitudinal and transverse weights $w_L(T), w_T(T)$ with best fit (see text); c) longitudinal relaxation rate, T_1^{-1} , vs. temperature; the solid line is the best fit to a simple model [16].

specific feature appears below a SC transition. Magnetic order gives rise to

$$\mathcal{A}_Z(t) = a_L G_{zz}(t) + a_T G_{xx}(t) \cos(2\pi\gamma B_i t), \quad (1)$$

distinguishing the longitudinal ($\mathbf{B}_i \parallel \mathbf{S}_\mu$, amplitude a_L) and the transverse ($\mathbf{B}_i \perp \mathbf{S}_\mu$, amplitude a_T) components, referred to the internal field \mathbf{B}_i . A simple geometric argument predicts a longitudinal weight $w_L = a_L/a_{ZF} = 1/3$ and $a_L + a_T = a_{ZF}$ for polycrystalline samples. If only part of the sample is magnetically ordered the weight $w_L = a_L/a_{ZF} > 1/3$ and one can evaluate the volume fraction in which muons experience the field \mathbf{B}_i as $f = 3a_T/2a_{ZF}$.

The combination of the two experiments on our superconducting samples, Y_{9–24}, yields a complete picture of their low temperature electronic properties.

The presence of *static* magnetism in superconducting samples is demonstrated by the appearance of strong magnetic relaxations in the ZF asymmetries and by their quenching in longitudinal fields larger than a few tens of mT. A clear example is given by sample Y₁₅, with zero resistance at $T_c = 30(1)$ K and $h = 0.070(1)$, whose normalized asymmetry \mathcal{A}_Z/a_{ZF} at $T = 1.3$ K (Fig. 1a) displays a very fast Gaussian relaxing transverse component, which is the signature of a distribution of sizeable static internal fields. The best fit yields two Gaussian contributions of standard deviation $\sigma/2\pi\gamma = (\overline{B^2} - \overline{B^2})^{1/2} = 25$ mT and 5 mT respectively [25], which correspond roughly to the coherent internal fields at the two muon stopping sites measured in the AF phase [15, 17]. Below T_N the longitudinal weight, w_L , is very close to the 1/3 value expected for a fully ordered material (see dashed curves in Fig. 1a). This proves the

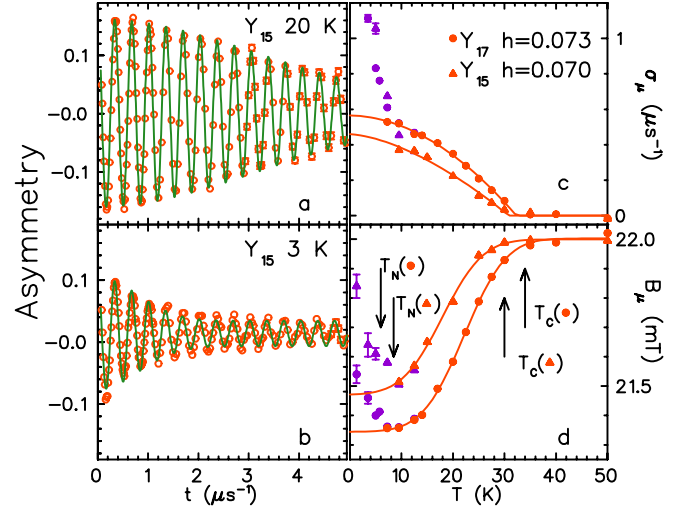


FIG. 2: TF μ SR data ($\mu_0 H = 22$ mT). Asymmetry a) for $T_N < T = 20\text{K} < T_c$ and b) for $T = 3\text{K} < T_N$ in sample Y₁₅; solid curves are best fits to a Gaussian damped precession. c) Relaxation rate σ_μ and d) internal field B_μ from the best fits for samples Y₁₅ and Y₁₇

presence of local magnetic moments (presumably in AF local structure) throughout the whole sample, although it cannot exclude the simultaneous presence of superconducting carriers to which ZF μ SR is insensitive.

The magnetic transition temperature is signaled by the appearance of a peak in the longitudinal relaxation rate T_1^{-1} , shown in Fig. 1c and obtained from a fit to Eq. 1 with $G_{zz} = \exp(-t/T_1)$. This relaxation corresponds to the slowing down of spin dynamics, due either to critical fluctuations (at the Neél temperature T_N) or to the freezing into a cluster spin glass state (at T_f). The two mechanisms are both present and distinct at lower doping [15], but here they cannot be told apart.

Figure 1b shows that the transverse weight $w_T(T)$ disappears above T_N , whereas the longitudinal weight $w_L(T)$ tends to unity. Their smooth dependence indicates the presence of a distribution of transition temperatures. The solid curves in the figure are a fit to a Gaussian distribution model [15], yielding $T_N = 7.8(2)$ K and a width of the distribution of $\Delta T_N = 2.1(2)$ K. The determinations of T_N , as from Fig. 1b ($w_L(T)$ and $w_T(T)$ fit) and Fig. 1c (T_1^{-1} peak), always agree within error bars.

The TF experiment on the very same sample quantifies the μ SR assessment of superconductivity. In the normal (paramagnetic) phase the local field B_μ coincides with $\mu_0 H$ and $G_{xx}(t)$ represents the weak Gaussian relaxation of width σ_n due to the random nuclear magnetic dipoles; in the superconducting phase a flux lattice is established and $G_{xx}(t) \approx \exp[-(\sigma_\mu^2 + \sigma_n^2)t^2/2]$ reflects the corresponding field distribution[18], approximated by a sizeable Gaussian decay parameter σ_μ . Figure 2a shows

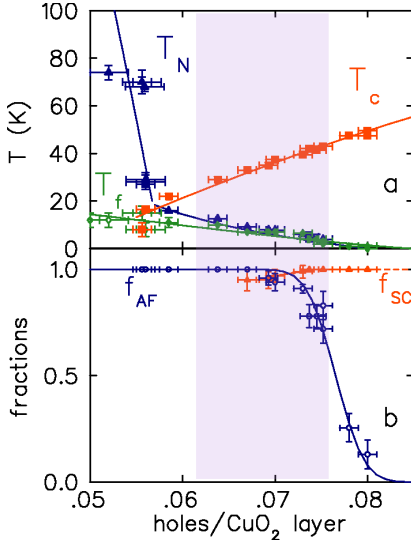


FIG. 3: Samples Y_{8-24} . a) Neél temperature T_N , freezing temperature T_f and critical temperature T_c vs. hole concentration h ; b) Muon volume fractions vs. h : AF (\circ , at $T = 0$ K) and SC (\blacktriangle , for $T_N \leq T \leq T_c$).

this damped precession.

The temperature dependence of the fitted parameters σ_μ and B_μ is shown in Fig. 2c and d, respectively, together with those of the slightly more doped Y_{17} sample ($h=0.73(1)$). They reveal the typical features of powder μ SR data in the SC state, including a clear diamagnetic shift of the local field $B_\mu = \mu_0 H(1 + \chi)$, with $\chi < 0$. The solid lines in Fig 2c are best fits to a BCS-like temperature power law [18] for $\sigma_\mu(T)$, $T > T_N$, which allows the extrapolation of the $\sigma_\mu(T = 0)$ value and the evaluation of the transition temperature $T_{c\mu}$, which coincides with T_c from zero resistance ($R(T) = 0$) within ± 1 K. The signal amplitude a_{SC} is very close to that of the normal phase (a_0 , for $T > T_c$), hence the volume fraction corresponding to the flux lattice signal may be calculated as $f_{SC} = a_{SC}/a_0$, with a value remarkably close to unity.

Spontaneous local fields \mathbf{B}_i appear for $T < T_N$. Since in polycrystalline samples they are randomly oriented with respect to $\mu_0 \mathbf{H}$, the vector composition $B_\mu = |\mu_0 \mathbf{H} + \mathbf{B}_i|$ leads to a spread of precession frequencies resulting in a much stronger damping of the asymmetry. The experimental data are shown in Fig. 2b with the same single Gaussian fit used for $T > T_N$ (solid line). The true lineshape is not Gaussian and a loss of initial asymmetry is also evident. However both $\sigma_\mu(T)$ and $B_\mu(T)$ (Fig. 2c,d) clearly reveal the onset of magnetic order.

Let us summarize at this point by stressing that *nearly all* muons detect *both* a flux lattice for $T_N < T < T_c$ and an internal AF field for $T < T_N$. Qualitatively similar results are obtained throughout the whole series of samples. Figure 3a shows the dependence of the two magnetic temperatures T_N and T_f upon hole content h across

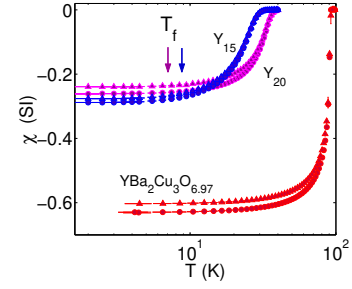


FIG. 4: SQUID susceptibility in $YBa_2Cu_3O_{6.97}$, Y_{15} ($h=0.70$) and Y_{20} ($h=0.75$): $H = 1$ O, FC (\blacktriangle) and ZFC (\bullet).

the coexistence region. As it was already mentioned they collapse into a single temperature for $h > 0.055$. Also shown is T_c corresponding to the midpoint of the SC transition measured by resistance $R(T)$). The smooth, continuous behaviour of all three temperatures demonstrates the well defined electronic properties of our samples and their high reproducibility.

The issue is whether bulk superconductivity survives below T_f . It may well, since the coherence length [19, 20] is $\xi \approx 80-200$ Å for $x = 0.60-0.57$, much larger than the characteristic length scale of the SC stripes mentioned above. Although the presence of SC below T_N might be retrieved from μ SR lineshape analysis, as it was attempted by modeling the complex internal field distribution in a single crystal [9], this is beyond the scope of our polycrystalline data and we reverted directly to SQUID magnetization measurements.

Figure 4 shows both field cooled (FC) and zero field cooled (ZFC) susceptibilities of Y_{15} , Y_{20} and of a $YBa_2Cu_3O_{6.97}$ sample, for reference, obtained as $\chi = M/(H - NM)$ in a low field $\mu_0 H = 0.1$ mT. We assumed $N = 1/3$ for the nearly spherical grain powders of average size $R \approx 1$ μm. We can neglect flux pinning since $\chi_{ZFC} \approx \chi_{FC}$. The field penetrates a spherical crust of thickness equal to the penetration depth λ and we expect $\chi = -f^3$ with $f = \lambda/R$, which is in good agreement [21] with the data. On these samples muons detect $T_N = 7.8(2), 4(1)$ K: the absence of magnetic contributions to χ on this scale is in agreement with an AF structure and with the low applied field. Since no change in the magnetization appears below T_N , the SQUID data also imply that the whole volume remains superconducting down to 2 K, well below T_N , which implies that superconductivity exists in this sample irrespective of the static nature of AF correlations.

The colored stripe in Fig. 3 shows the region where $T_N \approx T_f < T_c$. We evaluate the fraction of muons experiencing AF local fields, f_{AF} , from ZF experiments at the lowest temperature, as it is explained below Eq. 1. Likewise the amplitude a_{SC} in the TF experiments for $T_N < T < T_c$ yields the fraction f_{SC} of muons stopped in a SC environment. Figure 3b displays the two fractions,

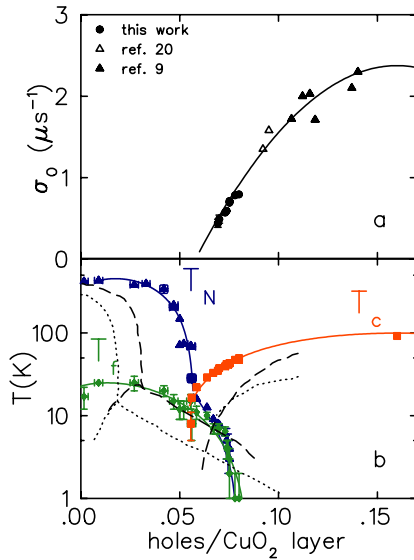


FIG. 5: $\text{YBa}_2\text{Cu}_3\text{O}_{6+x}$: a) muon Gaussian width σ_μ extrapolated to $T = 0$ vs. h ; b) phase diagram. Solid lines are guides to the eye, dashed ($\text{Y}_{1-y}\text{Ca}_y\text{Ba}_2\text{Cu}_3\text{O}_{6+x}$) and dotted ($\text{La}_{2-x}\text{Sr}_x\text{CuO}_4$) lines from ref. 5.

which are both close to unity for seven distinct samples ($\text{Y}_{14}\text{-Y}_{20}$) in a considerable portion of the colored area.

Note that $f_{AF} \approx 1$ does not imply that all Cu moments are ordered, rather merely that each muon site experiences some local magnetic field, i.e. that all implanted muons are within a short distance from static magnetic moments, since the dipolar fields fall as r^{-3} . This distance is typically estimated [5, 9] as $d \approx 20$ Å. The non magnetic volume fraction compatible with our observation of $f_{AF} \approx 1$ depends strongly on the cluster shape. For circular clusters [9] the upper limit is 0.2, while for stripe-like clusters it could be much larger, $\approx 1 - a/d$, where $a = 3.8$ Å is the lattice spacing. The latter case is compatible with our findings: Fig. 3b requires that a large fraction of muon sites are within a flux lattice for $T_N < T < T_c$ and the same sites experience a spontaneous internal field \mathbf{B}_i below T_N . This implies that both AF and SC domains belong to a superstructure, i.e. that they coexist at a nanoscopic scale, like in a short range order version of a stripe phase, with a percolating SC infinite cluster.

Figure 5b shows the full phase diagram for $\text{YBa}_2\text{Cu}_3\text{O}_{6+x}$, including our older data. From this plot the critical hole density for superconductivity is $h_c = 0.055(3)$. Note that $T_f(h)$ extrapolates to zero around $h = 0.082(3)$, a much lower value than those of $\text{La}_{2-x}\text{Sr}_x\text{CuO}_4$ and $\text{Y}_{1-y}\text{Ca}_y\text{Ba}_2\text{Cu}_3\text{O}_{6+x}$, and very far from the optimal SC value $h = 0.16$. This agrees with the larger distance between active and charge reservoir layers in the case of $\text{YBa}_2\text{Cu}_3\text{O}_{6+x}$, which reduces the influence of ionic disorder on magnetism and it suggests the lack of a causal link between AF and SC properties.

The appearance of local internal fields at all muon sites implies nm distance between AF stripes, while superconductivity requires a domain size larger than $\xi \gtrsim 10$ nm. How can these two geometrical constraints coexist? Only if AF correlations and SC pairing do not interfere. Metallic clusters nucleate in stripe form already at very low doping [15, 22]. AF cluster spin glass order survives above the critical metallic percolation threshold h_c , which corresponds to SC onset, probably because disorder frustrated AF correlations are harmless to SC pairing.

Finally the dependence of the muon width $\sigma_\mu(T = 0)$ upon h is plotted in Fig. 5a, together with a selection of results for higher dopings from ref. 9, 20 and references therein. The penetration depth $\lambda \propto (n_s/m)^{-\frac{1}{2}}$ may be extracted from the width ($\sigma_\mu = 7.58 \cdot 10^{-8} \lambda^{-2}$ in SI units [23]), hence, neglecting the variation of the effective mass m , the data show the dependence of the density of supercarriers n_s on h . Our data confirm the parabolic decrease of $n_s(h)$ down to very small values of $h - h_c$. Our data are also in agreement with the linear portion of the Uemura-plot [24], thanks to the parabolic shape [14] of T_c vs. h . The largest measured value of $\lambda(h)$ is $410(20)$ nm for $h = 0.070(1)$.

In conclusion we have demonstrated that a nanoscopic coexistence of static stripe-like magnetism and superconductivity takes place in $\text{YBa}_2\text{Cu}_3\text{O}_{6+x}$ as well. We have carefully mapped the phase diagram and complemented earlier measurements of $\lambda(h)$. Our observation of bulk superconductivity in Y_{15} and Y_{20} below the onset of spontaneous AF internal fields throughout most of the sample suggests that AF order and SC show minimal interference. In view of the nanoscopic coexistence of AF and SC domains it seems that the AF strings are almost transparent for superconducting carriers, which in our view reduces the plausibility for any *magnetic* model of high temperature superconductivity.

We gratefully acknowledge the support of G. Del Fiacco in sample preparation and characterization. We thank G. Guidi and M. Riccò for many fruitful discussions. RDR acknowledges financial support by FIRB project *Materiali magnetici innovativi strutturati su scala nanoscopica*.

-
- [1] J. H. Brewer *et al.*, Phys. Rev. Lett. **60**, 1073 (1988).
 - [2] A. Weidinger *et al.*, Phys. Rev. Lett. **62**, 102 (1989).
 - [3] D. R. Harshman *et al.* and A. Weidinger *et al.* reply, Phys. Rev. Lett. **63**, 1187-8 (1989).
 - [4] R. H. Heffner *et al.* and A. Weidinger *et al.* reply, Phys. Rev. Lett. **63**, 2538-9 (1989).
 - [5] Ch. Niedermayer *et al.*, Phys. Rev. Lett. **80**, 3843 (1998).
 - [6] A. Kanigel *et al.*, Phys. Rev. Lett. **88**, 137003 (2002).
 - [7] A. Keren and A. Kanigel, Phys. Rev. B **68**, 12507 (2003).
 - [8] C. Panagopoulos *et al.*, Phys. Rev. B **66**, 064501 (2002).

- [9] A. T. Savici *et al.*, Phys. Rev. B **66**, 174434 (2002).
- [10] H. A. Mook *et al.*, Phys. Rev. Lett. **88**, 097004 (2002).
- [11] S-W. Cheong *et al.*, Phys. Rev. Lett. **67**, 1791 (1991).
- [12] K. Yamada *et al.*, Phys. Rev. B **57**, 6165 (1998).
- [13] P. Manca *et al.*, Phys. Rev. B **63**, 134512 (2001).
- [14] J. Tallon *et al.*, Phys. Rev. B **51**, 12911 (1995).
- [15] S. Sanna *et al.*, Solid State Comm. **126**, 85 (2003).
- [16] N. Blöemberger *et al.*, Phys. Rev. **73**, 679 (1948).
- [17] H. Glückler *et al.*, Phys. Rev. **73**, 679 (1948).
- [18] B. Pümpin *et al.*, Phys. Rev. B **42**, 8019 (1990).
- [19] J. E. Sonier *et al.*, Phys. Rev. Lett. **79**, 2875 (1997).
- [20] R. I. Miller *et al.*, Physica B **326**, 196 (2003).
- [21] S. Sanna *et al.*, unpublished.
- [22] F. Borsa *et al.*, Phys. Rev. B **52**, 7334 (1995).
- [23] W. Barford and J. Gunn, Phys. C. **156**, 515 (1988).
- [24] Y. J. Uemura *et al.*, Phys. Rev. Lett. **66**, 2665 (1991).
- [25] At the lowest temperatures an overdamped precession may be alternatively fitted to the data, with similar quantitative conclusions.